# Evaluation of the radon adsorption efficiency of activated carbon fiber using tetrafluoromethane

Kotsar, Y.
Nakano, Y.
Takeuchi, Y.
Miuchi, K.

(Citation)
Progress of Theoretical and Experimental Physics,2022(2):023H01

(Issue Date)
2022-02

(Resource Type)
journal article

(Version)
Version of Record



(URL)
https://hdl.handle.net/20.500.14094/90009028

PTEP

Prog. Theor. Exp. Phys. **2022** 023H01(15 pages)
DOI: 10.1093/ptep/ptac005

# Evaluation of the radon adsorption efficiency of activated carbon fiber using tetrafluoromethane

Y. Kotsar[1], Y. Nakano[2], Y. Takeuchi[1,3,⋆], and K. Miuchi[1]

[1]*Department of Physics, Graduate School of Science, Kobe University, Kobe, Hyogo 657-8501, Japan*
[2]*Kamioka Observatory, Institute for Cosmic Ray Research, The University of Tokyo, Gifu 506-1205, Japan*
[3]*Kavli Institute for the Physics and Mathematics of the Universe (WPI), The University of Tokyo Institutes for Advanced Study, The University of Tokyo, Kashiwa, Chiba 277-8583, Japan*
⋆E-mail: takeuchi@phys.sci.kobe-u.ac.jp

Received November 22, 2021; Revised January 7, 2022; Accepted January 10, 2022; Published January 12, 2022

The radioactive noble gas radon-222 ($^{222}$Rn) is one of the most significant background sources in various types of rare event experiments, such as direct dark matter searches, neutrinoless double-beta decay searches, and neutrino experiments. Previously, a method to measure $^{222}$Rn concentration in purified air, argon, and xenon gases at a level of 1 mBq/m$^3$ was established. Since other detector media are used in these experiments, there is a potential need to expand the study for other types of gases. In this paper the performance of an 80 liter $^{222}$Rn detector filled with tetrafluoromethane ($CF_4$) gas, which is used for a direct dark matter search experiment, NEWAGE, was measured. The calibration factor of the detector for the $CF_4$ gas was measured and its dependence on the absolute humidity was investigated. We also employed activated carbon fiber to evaluate its $^{222}$Rn adsorption efficiency in $CF_4$, which was found to be $82.7 \pm 0.1(\text{stat.}) \pm 2.3(\text{syst.})\%$ at 0.10 MPa. For pressures lower than atmospheric pressure, we found that adsorption efficiency rises with lower pressure, and it is equal to $93.7 \pm 0.3(\text{stat.}) \pm 3.9(\text{syst.})\%$ at 0.03 MPa.

Subject Index H20

## 1. Introduction

### 1.1 *Dark matter search experiments*

Various approaches are used to detect dark matter in a wide mass range in direct and indirect searches, as well as in collider experiments. In recent years, however, the possible mass range for dark matter particle models has been refined extensively, and evidence points more in favor of cold dark matter [1,2]. Weakly interacting massive particles (WIMPs) are one of the candidates for cold dark matter. WIMPs are well motivated by cosmological findings [3,4] and supported by supersymmetry models, along with a universal extra dimension and little Higgs models [5–7]. In theories with WIMPs, their direct detection is achieved by looking for elastic WIMP–nuclei scatterings or WIMP–electron scatterings. For example, the XENON experiment, which consists of a time projection chamber with dual-phase xenon, set a world-leading constraint ($4.1 \times 10^{-47}$ cm$^2$ at 30 GeV) on the spin-independent elastic scattering cross-section in 2018 [8]. The expected event rate for these interactions is extremely low due to the small scattering cross-section, and accordingly, in order to distinguish these signals from the background, an additional characteristic signal other than the simple energy spectrum is needed. To that end, some dark matter experiments search for annual modulation of the event rate of the

aforementioned scatterings from the rotation of the Earth around the Sun, assuming dark matter has a uniform distribution throughout the Solar System. However, even these sets of data are not enough consistent among different dark matter search experiments. Another method is then required to obtain more robust evidence.

One such method is to measure the WIMP–nuclei scatterings relative to the Solar System's movement in the galaxy. If dark matter truly permeates the Milky Way, we would expect a flow of dark matter particles from the direction of the Cygnus constellation, which is in the forward direction of the Solar System's motion around the galactic center. NEWAGE (NEw generation WIMP search with an Advanced Gaseous tracking device Experiment) [9] is a direct dark matter search experiment located at the Kamioka Observatory, the Institute for Cosmic Ray Research (ICRR), the University of Tokyo. The experiment searches for a difference in recoil angle between events in the direction of the Cygnus constellation and in the opposite direction. It is thus a direction-sensitive experiment, and employs a gaseous three-dimensional fine tracking device (micro-TPC) that has a two-dimensional readout array, called the Micro Pixel Chamber ($\mu$-PIC) [10,11]. A gas electron multiplier is positioned above the $\mu$-PIC and helps to reach a sufficient intensity for readout [12].

### 1.2 *$CF_4$ in dark matter experiments*

Tetrafluoromethane ($CF_4$) is a structurally simple chemical compound with a low boiling point ($-127.8\,^{\circ}C$). It is sometimes used as a refrigerant, and can prepared by fluorination of carbon dioxide, carbon monoxide, or phosgene with sulfur tetrafluoride. Of particular interest, however, is its remarkable bond strength, owing to fluorine's high electronegativity and multiple carbon–fluorine bonds, which are the strongest in organic chemistry [13]. This property makes them a good quenching gas choice in neutron detectors [14], target material for neutrino detection [15], and a carrier gas in dark matter search experiments, such as the NEWAGE experiment [9] or the DRIFT experiment [16]. In particular, $CF_4$ is the target in the NEWAGE experiment since its fluorine nuclei have a large scattering cross-section for spin-dependent WIMP–nucleus interactions in extensions of the Standard Model of particle physics with WIMPs [17].

### 1.3 *Radon background in low-energy experiments*

In rare event search experiments, the background events from radioactive contaminants must be kept at a particularly low level. Such background sources include the noble gas in the uranium series, radon-222 ($^{222}$Rn), which has a half-life of 3.82 days and is produced continuously from trace amounts of radium-226 ($^{226}$Ra) in the detector material. Due to its relatively long lifetime, some persists in experiments and can mimic signals in the analysis-sensitive region. Therefore, the removal of $^{222}$Rn is a high priority in this class of experiments.

To that end, a $^{222}$Rn detector is first needed to measure $^{222}$Rn concentration with high accuracy and precision, since rare event search experiments usually require considerably low $^{222}$Rn concentrations. Although in this type of experiment measurements of $<1$ mBq/m$^3$ are required, there are currently no suitable commercially available Rn detectors, and so a special $^{222}$Rn detector has been developed for this purpose [18].

Since this type of experiment involves high-accuracy measurements, it is necessary to account for any dependent behavior in the Rn detector in order to consistently monitor the background level in the carrier gas. That includes the functional dependence of conversion factors between the measured variables and $^{222}$Rn concentration on those variables and/or external parameters.

Furthermore, a typical Rn detector employs a carrier gas, and in order to understand which gas would best perform in a particular experiment, quantitative analyses of different gases are required. In this study we evaluate the dependence of the calibration factor, which is the proportionality factor between the count rate in the detector and the $^{222}$Rn concentration, on the absolute humidity of the system for a $^{222}$Rn detector that employs $CF_4$. This dependence has already been analyzed for Rn detectors that employ purified air, argon (Ar) and Xe gases [18,19], but not for $CF_4$.

On the other hand, if $^{222}$Rn is to be removed, a quantitative analysis of its adsorption efficiency is needed to accurately predict how much $^{222}$Rn would be removed, and which removal method is valid to use in a particular experiment.

One method of $^{222}$Rn removal is to employ a trap which stores some material with high adsorption, such as activated carbon. This is charcoal, ingrained with micropores that significantly increase the surface area available for adsorption. For example, the NEWAGE detector uses a cooled charcoal trap in the gas circulation line to remove Rn in $CF_4$ [20]. It has also been found to be efficient at removing $^{222}$Rn from purified air, Ar, and Xe gases [21–23]. It is commonly used in pelletized, granular, powdered, or molded forms, but a new form—activated carbon fiber (ACF)—was developed in 1966 [24], and commercialized for use in water purification and surface treatment since the 1990s [19]. ACF is a powerful adsorbent due to its large surface area and low intraparticle diffusion, meaning smaller and more flexible sizes of its units in practice. However, ACF's application to removing $^{222}$Rn in purified gases has not been explored, expect for the case of $^{222}$Rn in purified air, Ar, and Xe [25,26]. In this paper we aim to evaluate the Rn adsorption efficiency of ACF in $CF_4$.

The surface of ACF contains numerous micropores, with a typical size of several nanometers. When a free particle gets close to the entrance of a micropore, a potential difference is induced due to the attraction term ($r^{-6}$) of the Lennard-Jones potential, and the particle is adsorbed at the surface of the pore due to the van der Waals forces. Since this term is sharp, the size of the adsorbed particle must be close to the pore size for this attraction to prevail, hence the nanometer pore size.

This paper is organized as follows. In Sect. 2 we evaluate the properties of an 80 liter (L) $^{222}$Rn detector [18] and describe the calibration system used in this study. In Sect. 3 we measure the calibration factor of this detector, which is the proportionality factor between the count rate in the detector and $^{222}$Rn concentration, and analyze its dependence on the absolute humidity. We also evaluated the background rate for a $^{222}$Rn detector filled with $CF_4$ gas. In Sect. 4 we evaluate Rn adsorption efficiency using ACF in $CF_4$ at different pressures lower than atmospheric pressure and measure its pressure dependence. In Sect. 5, we discuss the properties of the calibration factor for different gases and the Rn adsorption efficiency of ACF in different gases. The last section summarizes the results and gives future prospects for study.

## 2. Experimental setup

### 2.1 *Overview*

Previously, an 80 L $^{222}$Rn detector was developed for the use in high-accuracy low-energy experiments such as underground particle physics or low-energy dark matter experiments [18,27,28]. The detector system we used in this study is one of the calibration systems in Ref. [25], located at Kobe University. This calibration system is shown in Fig. 1 and consists of (1) a $^{222}$Rn source

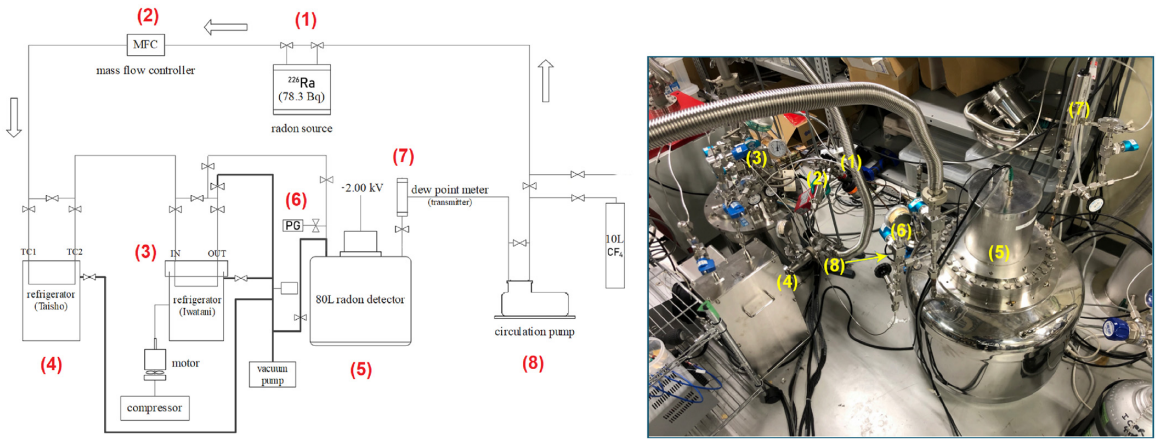


**Fig. 1.** Left: The detector system at Kobe University. Right: Photo of the system with the corresponding elements numbered.

(a Pylon Electronics PYLON RNC $^{226}$Ra container with radioactivity of 78.3 Bq), (2) a mass flow controller (Horiba SEC-Z500X), (3) a refrigerator to control the dew point temperature (Iwatani CryoMini PDC08), (4) a cold trap refrigerator (Taisho TC0147), (5) an 80 L $^{222}$Rn detector, (6) a pressure gauge (Swagelok P/N PGU-40-0C30-C-4FSM), (7) a dew point meter (Vaisala DMT152), and (8) a circulation pump (Enomoto Micro Pump Mfg. Co., Ltd. MX-808ST-S). The pressure gauge and the dew point meter are connected to the detector.

In Sect. 3, the cold trap refrigerator (4) was bypassed. In both the Rn adsorption efficiency experiments (Sect. 4), we used 10 g of ACF (A-25, produced by Unitika Ltd.), housed inside the cold trap, its refrigerator connected to the system. The type A-25 was chosen since this type was already tested in a previous study and its properties were evaluated in Xe gas [25].

## 2.2 *High-sensitivity $^{222}$Rn detector*

In our setup, we employ an 80 L $^{222}$Rn detector with a diameter of 500 mm. It has a stainless steel body with ICF (knife-edge) flanges, covered by a metal gasket. In order to reduce the self-contamination background from the detector's surface, electropolishing was carried out during production. The detector surface is grounded. The top part consists of a high-voltage divider and amplifier circuit [29], followed by a ceramic feed-through, which is set to rest on stainless steel plates. The circuit is connected to an 18 × 18 mm PIN photodiode (HAMAMATSU S3204-09) that hangs in the top center point of the vessel. This detector uses purified gases; in this study, we used $CF_4$ (purity 99.999%).

Once the carrier gas is released into the detector, $^{222}$Rn is expected to be mixed with it, and hence some decay patterns start appearing inside the detector, given that the intrinsic background of the vessel is lower than the $^{222}$Rn concentration. By applying a reverse-bias negative high voltage to the photodiode and creating an electric field between the photodiode and the vessel, different cations from down the decay chain of $^{222}$Rn start drifting towards the photodiode, and are electrostatically collected and read out at the circuit board in different analog-to-digital converter (ADC) channels. We chose −2.0 kV as the high-voltage value for our measurements with $CF_4$.

Two peaks are prominent in the pulse height spectra for this detector and are visible in Fig. 2. They correspond to $^{218}$Po (6.11 MeV) and $^{214}$Po (7.83 MeV). In this study we used the signal

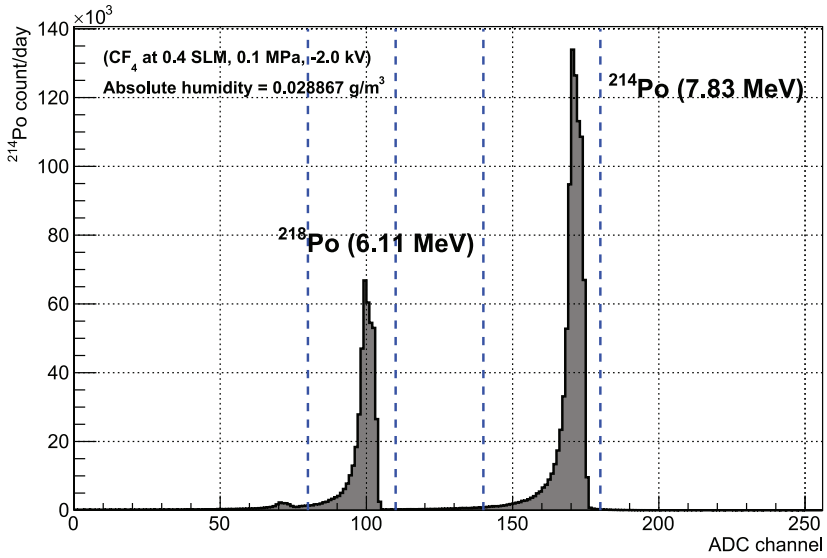


**Fig. 2.** Characteristic pulse height spectrum for $^{214}$Po and $^{218}$Po daily count rates, with the integration windows shown in blue vertical lines. The experimental conditions are shown at the top left.

from $^{214}$Po for the integrated count rate, since $^{214}$Po exists in a lower stream of the decay chain, and hence the $^{222}$Rn detector has a higher collection efficiency for $^{214}$Po. In addition, while there is a $^{212}$Bi peak (6.21 MeV) close to the $^{218}$Po energy peak, there are no other alpha sources whose energy peaks overlap with that of $^{214}$Po. The integration range for the count rate was set from 140 to 180 (ADC channels) to maximize $^{214}$Po detection efficiency, similar to how it was done in Ref. [27]. The settings of the voltage amplifier affect the peak positions. We checked before each dependence measurement that the peak positions were the same, and therefore the integration range is still appropriate.

## 3. Calibration factor analysis

### 3.1 *Measurement system for calibration factor*

It is known from previous studies that the calibration factor of a $^{222}$Rn detector depends on the humidity of the contained gas [18]. This stems from the fact that, while drifting to the photodiode, $^{214}$Po and $^{218}$Po ions have a non-zero chance to scatter off water molecules contained in the gas and undergo neutralization [30]. This partial neutralization of Po ions in the vessel results in a lower count rate in high-humidity gas. The decrease in the rate of Po ions collected electrostatically should be accounted for in the calibration factor. Phenomenological analysis predicts that this decrease (neutralization rate) for small ions is proportional to the square root of the humidity [31]. In a similar way in Ref. [27], the calibration factor was found to be best described by a negative square root dependence on the absolute humidity for other gases (purified air, Ar, and Xe).

For our analysis of the calibration factor's dependence on absolute humidity we used the system described in Sect. 2.1, but with only one refrigerator to control the dew point temperature (the cold trap refrigerator was bypassed). By specifying a setpoint temperature, the refrigerator will stabilize the system to a dew point temperature of approximately the same value within 20 hours on average. From there, we can calculate the absolute humidity for a known dew point (see Appendix).

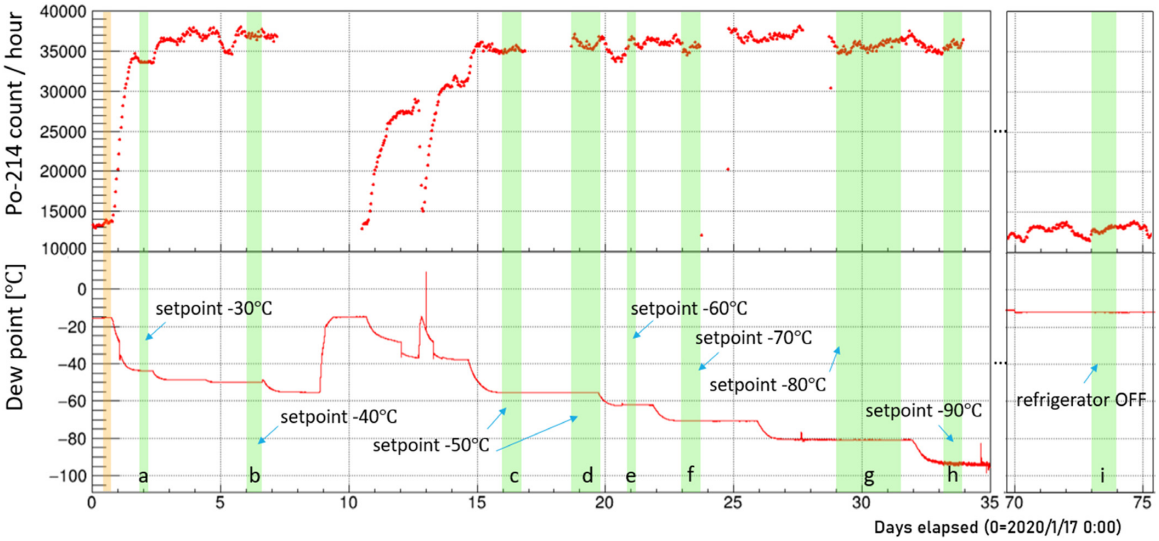


**Fig. 3.** Time variation of the $^{214}$Po count rate and the dew point temperature in the detector filled with $CF_4$, along with the nine analyzed data ranges (shown in green, marked by letters from a to i), corresponding to setpoint values from $-90\,^{\circ}$C to room temperature). The range shown in orange is the short period before the refrigerator was turned on that was additionally analyzed.

The calibration factor ($C_F$) was calculated in the following way:

$$C_F\ [(\text{count/day})/(\text{Bq/m}^3)] = \frac{\text{ADC count [count/day]}}{\text{expected } ^{222}\text{Rn concentration [mBq/m}^3]}, \tag{1}$$

where the ADC count is measured by the Rn detector and the expected $^{222}$Rn concentration is calculated from the activity of the Rn source and the volume of the calibration system: $^{222}$Rn concentration $= 78.3\,\text{Bq}/0.08\,\text{m}^3 = 978.7\,\text{Bq/m}^3$ under radioactive equilibrium.

### 3.2 *Humidity dependence*

Before starting the measurements, the inside of the detector was sufficiently vacuumed with the turbomolecular vacuum pump shown at the bottom in Fig. 1(left). In our study, the flow rate was set to 0.4 standard liters per minute (SLM) using the mass flow controller. Next, $CF_4$ was introduced into the system. The refrigerator was turned on, its setpoint was set to $-30\,^{\circ}$C, and the dew point temperature allowed half a day to stabilize. A period where the dew point temperature is approximately constant was selected, and the average value of the $^{214}$Po count rate was calculated for that period in order to determine the calibration factor. It was then converted to the calibration factor using Eq. (1). In our analysis of humidity dependence, we used a constant $^{222}$Rn concentration (under radioactive equilibrium), calculated from the radioactivity of the source and the detector volume. This procedure was performed for eight setpoint values, for which nine periods in total were selected (two periods were selected for a setpoint at $-50\,^{\circ}$C). The last data range was obtained with the refrigerator turned off (room temperature was $+25\,^{\circ}$C, corresponding to a dew point in $CF_4$ of approximately $-11\,^{\circ}$C). The time variation of the $^{214}$Po count rate (per hour) and the dew point temperature are shown in Fig. 3. We additionally calculated the calibration factor for a short period before the refrigerator was turned on (days 0.44–0.71). However, this period is too short for an accurate average $^{214}$Po count value, since there is the possibility of the $^{214}$Po count being unstable, and thus we calculated the

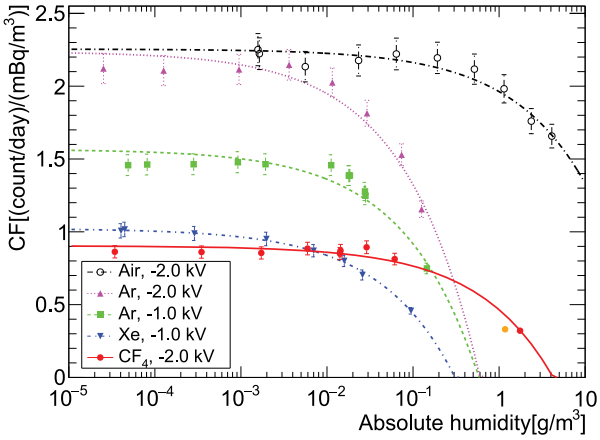


**Fig. 4.** Calibration factor of the 80 L $^{222}$Rn detector as a function of the absolute humidity for $CF_4$ and other gases: purified air (black) [27], Ar (pink and green), Xe (blue), and $CF_4$ (red) [18]. The vertical error bars for $CF_4$ include the statistical and systematic errors described in Table 1. The one point drawn in orange is the calibration factor calculated from the short period before the refrigerator was turned on.

conversion factor using the data taken during this period, while we excluded this data from the absolute humidity dependence.

Figure 4 shows the resulting calibration factor as a function of absolute humidity for the case of $CF_4$, along with the results for other gases [18,27]. The fitted function for the case of $CF_4$ is given by

$$C_F = -0.44\sqrt{AH} + 0.90, \tag{2}$$

where $AH$ is the absolute humidity in the gas (g/m$^3$). This demonstrates that the calibration factor of $CF_4$ gas clearly depends on its humidity with a negative square root functional form similar to other gases. The calibration factor has a flat region for $AH$ below $10^{-2}$ g/m$^3$, but drops to half its value at an $AH$ around 1 g/m$^3$.

Typical values of the calibration factor (data regions h (setpoint at $-90\,^\circ$C) and i (refrigerator off) in Fig. 3) at specified absolute humidities, with the systematic uncertainties described below, were

$$C_F \text{ (region h)} = 0.87 \pm 0.10\,\text{(count/day)/(mBq/m}^3\text{)} \text{ at } 3 \times 10^{-5}\,\text{g/m}^3,$$
$$C_F \text{ (region i)} = 0.33 \pm 0.04\,\text{(count/day)/(mBq/m}^3\text{)} \text{ at } 1.75\,\text{g/m}^3.$$

For the calibration factor measurements, the systematic uncertainties were estimated in the same way as in Ref. [18]. The uncertainties come from the accuracy of the radioactivity of the $^{222}$Rn source (±4.0%), the accuracy of the dewpoint meter (±2.0%), and the accuracy of the estimation of the total volume of the calibration system, including the 80 L detector and vacuum tubing (±2.0%). All of the accounted uncertainties are presented in Table 1.

### 3.3 *Background run*

Lastly, we measured the background level of the system by bypassing the $^{222}$Rn source and allowing the $^{222}$Rn in the system to decay. The gas flow was still maintained with the circulation pump at 0.4 SLM. After the decay, the $^{214}$Po count reached a constant rate. We measured it for 14.5 days and obtained an average rate of 1.24 ± 0.09(stat. only) count/day for the system background. The pulse height spectrum for this period is shown in Fig. 5.

**Table 1.** Systematic uncertainties on the calibration factor of a $^{222}$Rn detector with $CF_4$. The uncertainties marked with a † come from the technical specifications of each item.

| Cause | Uncertainty [%] |
|---|---|
| Accuracy of the radioactivity of the $^{222}$Rn source† | ±4.0 |
| Accuracy of the dewpoint meter† | ±2.0 |
| Accuracy of the total volume estimation of the calibration system | ±2.0 |

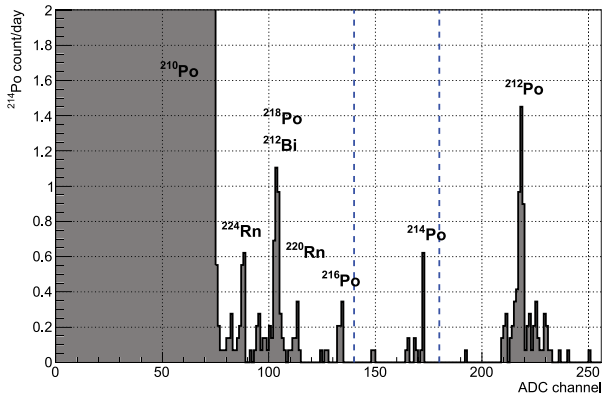


**Fig. 5.** The pulse height spectrum for the 14.5-day measurement of the background of a $^{222}$Rn detector filled with $CF_4$. $^{224}$Ra (5.79 MeV), $^{212}$Bi (6.21 MeV), $^{220}$Rn (6.40 MeV), $^{216}$Po (6.91 MeV), and $^{212}$Po (8.78 MeV) originate from the thorium decay series. These come from the inner surface material of the Rn detector and result in the intrinsic background of the Rn detector. The integration window of $^{214}$Po is shown in blue vertical lines.

We found some alpha sources originating from the thorium decay series, such as $^{224}$Ra, $^{212}$Bi, $^{220}$Rn, $^{216}$Po, and $^{212}$Po. Their spectra do not overlap with the $^{214}$Po signal region. Thus, the background measurement was appropriately performed without contamination from other alpha sources. Since this measurement was performed at the end of a 170-day decay of $^{222}$Rn, the count rate of $^{210}$Po in the background spectrum is high in comparison with other alpha sources. The increase is likely due to positively charged $^{210}$Pb from the $^{222}$Rn decay chain accumulating on the surface of the PIN photodiode over the measurement history of the detector. Since it decays with a half-life of 22 years to produce the observed $^{210}$Po, the increased count rate indicates that $^{222}$Rn daughters remain on the photodiode once they have been collected.

Comparing this measurement to previous measurements done on the same detector [18], where the background level was 0.81 ± 0.08(stat. only) count/day for purified air (−2.0 kV), the background level of $CF_4$ (−2.0 kV) is about 1.5 times as prominent. While the current measurement was done on the whole system, as opposed to previous measurements on the 80 L detector, the value is nonetheless acceptable and low enough to have negligible effects on the measurements in this study.

## 4. Rn adsorption efficiency of ACF

### 4.1 *Measurement system for Rn adsorption*

To evaluate the $^{222}$Rn adsorption efficiency of ACF we used the setup described in Sect. 2.1, with the cold trap refrigerator ((4) in Fig. 1). It contains a cold trap with the ACF.

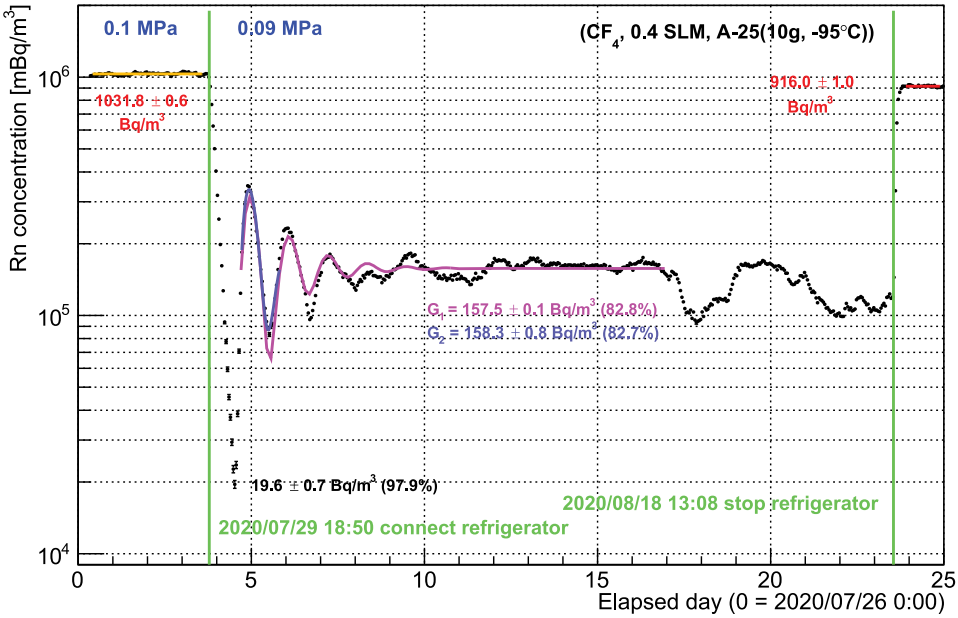


**Fig. 6.** $^{222}$Rn concentration variation in $CF_4$ in the Rn adsorption efficiency experiment. The orange and red lines show fitting results during the bypass and off phases, respectively. The fitting functions for methods (1) and (2) are shown by the magenta and blue lines, respectively. $G_1$ and $G_2$ are the values of the fitting parameter $G$ in methods (1) and (2). The experimental conditions are shown at the top.

We carried out two experiments: an adsorption test at atmospheric pressure and a pressure dependence experiment, with multiple tests at different pressure levels, with the Rn source bypassed.

### 4.2 *Evaluation at atmospheric pressure*

In this experiment, $CF_4$ gas was already circulating in the system. The initial temperature was room temperature (+25 °C). We call this the "bypass phase," since the cold trap refrigerator was bypassed. After the flow rate was fixed at 0.4 SLM, the cold trap refrigerator was set to a temperature of −95 °C and connected to the system, initiating the "adsorption phase." The measurements were carried out for 19.5 days before the refrigerator was turned off. Thus began the "off phase." In the "off phase," we collected data for a couple more days. Even though the refrigerator was turned off, the trap was still operational, and hence some of the original Rn was still trapped inside, lowering the $^{222}$Rn concentration for this region. The $^{222}$Rn concentration variation during the experiment is shown in Fig. 6. It was calculated from the integrated count rate for $^{214}$Po using the calibration factor function found in Sect. 3.2. We also observed a pressure drop of about 0.01 MPa in the adsorption phase.

The oscillatory pattern of the Rn concentration measured with the Rn detector is thought to correspond to the characteristic $^{222}$Rn adsorption behavior of the trap. This behavior is damped by the turbulence and longitudinal diffusion along the length of the trap [21]. The time in which the $^{222}$Rn concentration damps out and becomes stable varies with the flow rate in the system. In this study, all measurements were performed at 0.4 SLM. The stabilization time for these conditions was found to be around 7.5 days. Note that there was still some turbulence after the oscillation had dampened out, which is the random turbulence due to the stochastic nature of the cold trap.

**Table 2.** Comparison of evaluation methods for $^{222}$Rn adsorption efficiency in $CF_4$. The systematic errors are obtained from Table 3.

| Evaluation method | $^{222}$Rn concentration [Bq/m$^3$] | Adsorption efficiency [%] |
|---|---|---|
| Method (1): long fitting region | $157.5 \pm 0.1$(stat.) | $82.8 \pm 0.1$(stat.)$\pm$2.2(syst.) |
| Method (2): short fitting region | $158.3 \pm 0.8$(stat.) | $82.7 \pm 0.1$(stat.)$\pm$2.3(syst.) |

We calculated the adsorption efficiency ($E_{\text{ads}}$) by comparing the $^{222}$Rn concentrations in the off phase (at $+25\,^{\circ}$C) and in the adsorption phase (at $-95\,^{\circ}$C):

$$E_{\text{ads}} = \frac{C_{\text{off}} - C_{\text{adsorbed}}}{C_{\text{off}}} \times 100.0\,[\%], \tag{3}$$

where $C_{\text{off}}$ ($C_{\text{adsorbed}}$) is the Rn concentration in the off (adsorption) phase.

We evaluated the concentration in the adsorption phase by fitting with a damped sinusoidal function of the form $f(t) = A \cdot e^{-Bt}\sin(Dt + F) + G$, where $t$ is the elapsed day, in the region of interest: starting after the first oscillation minimum and including the oscillation and the whole stable region after it. Since the asymptote for the function $f(t)$ is $G$, we used the value of $G$ as $C_{\text{adsorbed}}$ in method (1) in Table 2. We then performed another fit with free parameters for the same function $f(t)$ with a narrower region. The fit was performed for the region between two data points with approximately the same Rn concentration value, but separated by about one period of oscillation including the first maximum and the second minimum of oscillation. We found a similar value of $G$, which is used in method (2) in Table 2. Furthermore, the difference between the concentration (and hence adsorption efficiency) values in methods (1) and (2) is sufficiently small to allow us to choose method (2) as the main method. Even though method (2) has a larger uncertainty, it is crucial for the evaluations in Sect. 4.3, where the time until $^{222}$Rn decays fully was limited, and it was not possible to wait for the whole stabilization period of 7.5 days multiple times to collect stable data in the adsorption phase.

We also calculated the efficiency at the oscillation minimum. This point indeed corresponds to the maximum adsorption efficiency: $E_{\text{ads}}(\text{osc. min.}) = 97.9 \pm 0.1(\text{stat.})\%$.

Next, we estimated the systematic uncertainties on the adsorption efficiency. Since the experimental setup used in Ref. [25] was similar, we inherited a $\pm 2.0\%$ reproducibility uncertainty. We also had an accuracy uncertainty of the analog pressure gauge of $\pm 0.001$ MPa, resulting in a pressure uncertainty between $\pm 1.0\%$ (at 0.10 MPa) and $\pm 3.3\%$ (at 0.03 MPa). We have also included the uncertainty associated with the choice of a fitting region in method (2). To evaluate the uncertainty, we performed two additional fits: we shortened and extended the boundary of the fitting region by one data point, respectively. From this analysis, the difference in the Rn concentration during the adsorption phase was obtained in the range of $-2.9\%$ (at 0.03 MPa) and $+9.3\%$ (at 0.03 MPa). Propagating this difference to the uncertainty on the adsorption efficiency resulted in a range of $-0.18\%$ (at 0.03 MPa) and $+0.59\%$ (at 0.03 MPa). The uncertainty due to the accuracy of the weighted fit is discussed in Sect. 4.3.

A summary of the systematic uncertainties on the $^{222}$Rn adsorption efficiency is shown in Table 3.

### 4.3 *Pressure dependence*

Next, we conducted an experiment to evaluate the pressure dependence of ACF's Rn adsorption efficiency. In a lot of dark matter search experiments (such as NEWAGE) it is necessary

**Table 3.** Systematic uncertainties on the $^{222}$Rn adsorption efficiency in $CF_4$.

| Cause | Uncertainty [%] |
|---|---|
| Accuracy of pressure | ±1.0 (at 0.10 MPa) ∼±3.3 (at 0.03 MPa) |
| Reproducibility | ±2.0 |
| Fitting region choice *(method (2) only)* | −0.18 ∼ +0.59 |
| Accuracy of the weighted fit *(Sect. 4.3 only)* | −0.23 ∼ +0.58 |

to operate with gases at low pressures. Therefore, in this experiment we tested whether the Rn adsorption efficiency is sufficient at low pressures.

Since this experiment continued from the experiment at atmospheric pressure (Sect. 4.2), $CF_4$ was already introduced in the system and the trap turned on. Before the measurement procedures, the cold trap refrigerator was baked at +85 °C and the inside of the detector was sufficiently vacuumed with the turbomolecular pump, as in Sect. 3.2. After baking, we lowered the temperature to room temperature. Since the Rn source employed cannot be used at low pressures, according to the specifications, it was then bypassed from the system, and data taking began. Shortly after that, we used the turbomolecular pump to lower the pressure level down to 0.08 MPa. After we left the system for sufficient time for fitting, we turned on the refrigerator, which brought the temperature down to −95 °C. This accelerated the adsorption process so that the characteristic oscillation pattern appeared in the $^{222}$Rn concentration, as shown in Fig. 7. Continuing the method from Sect. 4.3, in the activated (adsorption) region it was sufficient for us to collect data until about the second maximum. Finally, we turned the refrigerator off and allowed roughly the same amount of time to obtain data for fitting. These procedures were then repeated at 0.06 MPa, 0.04 MPa, and 0.03 MPa. The pressure levels were chosen to change from 0.10 MPa in steps of 0.02 MPa, with the exception of the last level, which due to the limitations of the circulation pump was set as 0.03 MPa.

Figure 7 shows four plots for the four different pressure values listed above. The $^{222}$Rn concentration in the plots is corrected for exponential decay by multiplying the concentration with the exponential law (using the half-life period for $^{222}$Rn of 3.82 days). This is done for easier comparison with the experiment at atmospheric pressure, and to show that this decay obeys the exponential law.

We fitted the oscillatory parts according to method (2) in Sect. 4.2 and determined $C_{\text{adsorbed}}$ for the four regions shown in Fig. 7, and performed constant fits in the "off phases" for the same four regions to obtain $C_{\text{off}}$. Their relation, calculated as in Eq. (3) (this time accounting for the decay), is the $^{222}$Rn adsorption efficiency. Figure 8 shows this efficiency for the four regions analyzed. The adsorption efficiency at 0.03 MPa is $93.7 \pm 0.3(\text{stat.}) \pm 3.9(\text{syst.})\%$. The results suggest that the $^{222}$Rn adsorption efficiency has an inverse relationship with the pressure. This was also shown to be the case for Xe gas [25].

Since the measurements in this experiment were performed one after another, it is expected that residual Rn exists in the trap, and this resulted in the different Rn concentrations before and after the adsorption phase. To take this into account, for each pressure level, the $^{222}$Rn concentration was fitted as one weighted fit of two stable regions– the "off phases" before and after the "adsorption phase." Note that there is no "bypass phase" this time, as the refrigerator

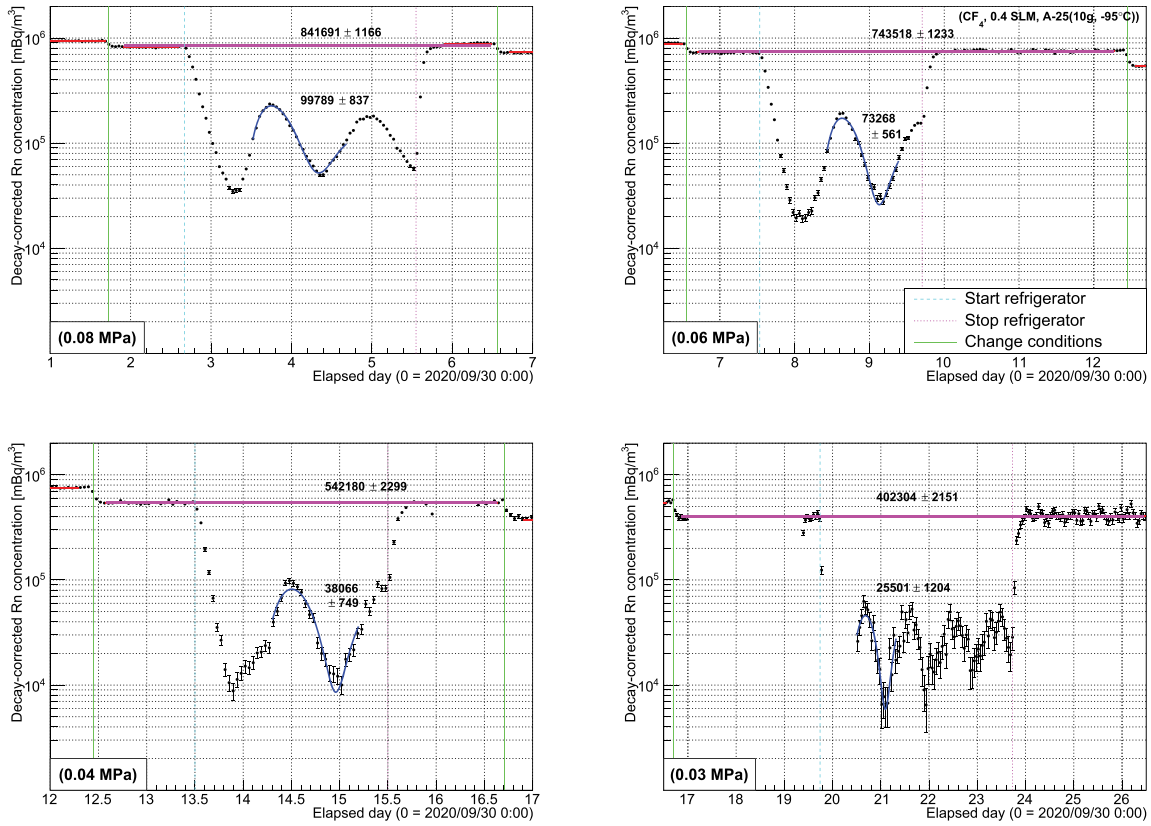


**Fig. 7.** Decay-corrected $^{214}$Po count at four different pressure values in the adsorption efficiency experiment using $CF_4$ gas. The operation times are shown with vertical lines, and the operations explained in the top right panel, along with the experimental conditions.

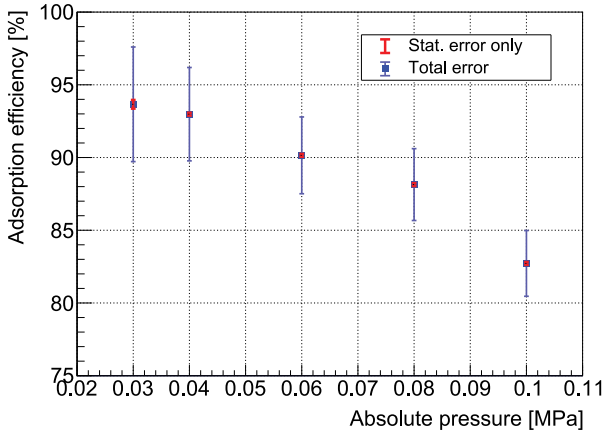


**Fig. 8.** $^{222}$Rn adsorption efficiency of ACF in $CF_4$ at $-95\,^{\circ}$C as a function of the absolute pressure. The vertical error bars in red are statistical error only. The vertical error bars in blue include the statistical and systematic uncertainties summarized in Table 3.

was connected during the whole pressure dependence experiment. The results from separate fits of these two regions show that there is a difference in concentration between the before and after "off phases." This difference ranges from $-2.1\%$ (at 0.03 MPa) to $+4.9\%$ (at 0.08 MPa). Propagating this difference to the uncertainty on the adsorption efficiency resulted in a range

**Table 4.** $\sigma$ parameters of the Lennard-Jones potential for different gases and Rn adsorption efficiency. $CF_4$ is the result presented in Sect. 4 of this paper.

| Gas type | $\sigma$ parameter [nm] | Rn adsorption efficiency [%] | Conditions |
|---|---|---|---|
| Ar | 0.340–0.346 [32] | $98.3 \pm 0.1$(stat.) $\pm$ 0.2(syst.) | 1.3 SLM, 0.1 MPa [25] |
| Air | 0.352–0.369 [32] | $97.9 \pm 0.1$(stat.) $\pm$ 0.2(syst.) | 0.9 SLM, 0.1 MPa [25] |
| Xe | 0.396–0.410 [32] | $27.8 \pm 0.2(\text{stat.})^{+2.0}_{-5.5}$(syst.) | 0.14 SLM, 0.1 MPa [25] |
| Rn | 0.417–0.421 [33] | — | — |
| $CF_4$ | ∼0.470 [32] | $82.7 \pm 0.1$(stat.) $\pm$ 2.3(syst.) | 0.4 SLM, 0.1 Pa |

of −0.23% (at 0.08 MPa) and +0.58% (at 0.08 MPa). We have included this as a systematic uncertainty for the adsorption efficiency in Table 3.

## 5. Discussion

### 5.1 *Calibration factor*

In the Lennard-Jones potential approximation, the particle size is represented by the $\sigma$ parameter. Table 4 summarizes the $\sigma$ parameters for different gases.

Comparing the cases where the applied high voltage is −2.0 kV (Fig. 5), we can see that the calibration factor for $CF_4$ is about half the calibration factor of the other gases. This could be explained by the difference in $\sigma$ parameters for the Lennard-Jones potential. Out of the gases for which the calibration factor's humidity dependence was explored so far, the $\sigma$ parameter of $CF_4$ is the largest (∼0.470 nm), since $CF_4$ is a polyatomic molecule. On the other hand, as previously discussed, some Po ions that are drifting towards the photodiode in the detector's volume have a non-zero chance to scatter off the carrier gas molecules (as well as the water molecules mixed within the gas). Having scattered, they undergo neutralization and fail to reach the photodiode surface, resulting in a lower count rate. Therefore, it could be speculated that the calibration factor depends also on the $\sigma$ parameter of the gas type employed.

### 5.2 *Rn adsorption efficiency of ACF*

It can be speculated that when the $\sigma$ parameter for particles of the carrier gas is close to the $\sigma$ parameter of $^{222}$Rn, a significant number of pores in the ACF will have these carrier gas particles adsorbed instead of $^{222}$Rn. This can be seen from the significantly low Xe adsorption rate in Table 4.

The obtained values for Rn adsorption efficiency in $CF_4$ (Fig. 8) could be explained by focusing on the inter-molecular interaction of gases near the surface of the ACF (Sect. 1.3). As summarized in Table 4, Xe gas has the lowest $^{222}$Rn adsorption efficiency. This is possibly due to the fact that a considerable proportion of the $^{222}$Rn atoms never have a chance to be adsorbed, as they are superseded by Xe atoms, which have the closest Lennard-Jones $\sigma$ parameter to $^{222}$Rn, and hence are a suitable size for adsorption.

On the other hand, the amplitude of the oscillations at the start of adsorption also varies with different carrier gases. Comparing with the results from Ref. [25], we can see that $CF_4$ has the greatest amplitude out of the sample. This is hypothesized to be related to the Lennard-Jones $\sigma$ parameter: a large $\sigma$ parameter would mean that the molecule is more likely to push an already residing molecule (in this case $^{222}$Rn) out of a pore. This pattern is unlikely to occur for smaller molecules (purified air and Ar gas), as we can see in Ref. [ 25] and Table 4.

## 6. Conclusion

$CF_4$ gas is widely used for particle detection in the field of particle physics because of its properties. We have evaluated the calibration factor for an 80 liter $^{222}$Rn detector and analyzed its dependence on the absolute humidity for the case of $CF_4$. We found a dependence on the absolute humidity described by the function $C_F(AH) = -0.44\sqrt{AH} + 0.90$, where $C_F$ is the calibration factor defined in Sect. 3.1. Its value was found to be about the same as the calibration factor for Xe gas, and about half the calibration factor for Ar gas and purified air, for $AH$ below $10^{-2}$ g/m$^3$, and with $-2.0$ kV applied.

In Sect. 4, we successfully employed ACF inside a cold trap to evaluate its Rn adsorption efficiency in $CF_4$. This was found to be $82.7 \pm 0.1(\text{stat.}) \pm 2.3(\text{syst.})\%$ at 0.10 MPa (against room temperature adsorption at $+25\,^\circ$C). For pressures lower than atmospheric pressure, namely between 0.10 MPa and 0.03 MPa, we saw that it similarly increases with a decrease in pressure, up to $93.7 \pm 0.3(\text{stat.}) \pm 3.9(\text{syst.})\%$ at 0.03 MPa. We speculate that the lower adsorption efficiency compared to other carrier gases can be explained by a difference in the $\sigma$ parameter in the Lennard-Jones potential. To investigate this further, we aim to carry out another experiment using a $28 \times 28$ mm PIN photodiode (HAMAMATSU, S3584-09) and a low-chemical-reactivity, low-electronegativity carrier gas with even closer molecular parameters to $^{222}$Rn. Owing to its larger resolution, a larger photodiode would provide greater collection efficiency, and hence less error on $^{222}$Rn concentration and Rn adsorption efficiency.

We have shown that at pressures lower than atmospheric pressure, ACF retains the ability to adsorb Rn in $CF_4$. In this regard, it is a good candidate for use at experiments such as the NEWAGE experiment.

**Acknowledgments**

The authors would like to thank Mr. Weiguang Gao, a research student at the Graduate School of Science, Kobe University, during 2019–2020, for his contribution on the measurement of the humidity dependence data. The authors would like to thank Unitika Ltd. for providing the ACF sample. This work is supported by Japan Society for the Promotion of Science (JSPS) KAKENHI Grant Numbers 26104005, 26104008, 18H05536, 19H05806, and 21K13942.

## Appendix. Empirical formula for absolute humidity

To calculate the absolute humidity in the carrier gas, we first need to know the saturated vapor pressure of ice, $P$ [kPa], which is given by the following formula [34]:

$$P = \exp\left(-\frac{6024.5282}{T_{\text{dew}}} + 29.3271 + 0.0106139\ T_{\text{dew}} + 0.0000132\ T_{\text{dew}}^2 - 0.4938258\ \ln T_{\text{dew}}\right). \tag{A1}$$

Here, the dew point temperature ($T_{\text{dew}}$) is in units of kelvin.

The formula for absolute humidity ($AH$ [g/m$^3$]) is a simple relation between $P$ and the air temperature ($T_{\text{air}}$ [$^\circ$C]) in the carrier gas:

$$AH = \frac{0.00794\ P}{1 + 0.00366\ T_{\text{air}}}. \tag{A2}$$

## References

[1] M. Kunz, S. Nesseris, and I. Sawicki, Phys. Rev. D **94**, 023510 (2016).
[2] N. Aghanim [Planck Collaboration] et al., A&A **641**, A6 (2020).
[3] V. C. Rubin and W. Kent Ford Jr, Astrophys. J. **159**, 379 (1970).

[4] L. D. Bradley et al., Astrophys. J. **678**, 647 (2008).
[5] G. Jungman, M. Kamionkowski, and K. Griest, Phys. Rep. **267**, 195 (1996).
[6] A. Birkedal, A. Noble, M. Perelstein, and A. Spray, Phys. Rev. D **74**, 035002 (2006).
[7] M. T. Arun, D. Choudhury, and D. Sachdeva, J. Cosmol. Astropart. Phys., **2017**, 041 (2017).
[8] E. Aprile [XENON Collaboration] et al., Phys. Rev. Lett. **121**, 111302 (2018).
[9] T. Tanimori, H. Kubo, K. Miuchi, T. Nagayoshi, R. Orito, A. Takada, and A. Takeda, Phys. Lett. B **578**, 241 (2004).
[10] T. Hashimoto et al., Nucl. Instrum. Meth. A **977**, 164285 (2020).
[11] A. Takada et al., Nucl. Instrum. Meth. A **573**, 195 (2007).
[12] F. Sauli, Nucl. Instrum. Meth. A **805**, 2 (2016).
[13] D. O'Hagan, Chem. Soc. Rev. **37**, 308 (2008).
[14] M.-K. Moon, U.-W. Nam, C.-H. Lee, V. T. Em, Y.-H. Choi, J.-K. Cheon, and K.-N. Kong, Nucl. Instrum. Meth. A **538**, 592 (2005).
[15] C. Amsler et al., Nucl. Instrum. Meth. A **396**, 115 (1997).
[16] E. Daw et al., Astropart. Phys., **35**, 397 (2012).
[17] S. Archambault et al., Phys. Lett. B **682**, 185 (2009).
[18] K. Hosokawa, A. Murata, Y. Nakano, Y. Onishi, H. Sekiya, Y. Takeuchi, and S. Tasaka, Prog. Theor. Exp. Phys. **2015**, 033H01 (2015).
[19] K. Tai and N. Shindo, Sen'i Gakkaishi **49**, P177 (1993).
[20] K. Nakamura et al., Prog. Theor. Exp. Phys. **2015**, 043F01 (2015).
[21] K. Abe et al., Nucl. Instrum. Meth. A **661**, 50 (2012).
[22] M. Ikeda, T. Hokama, S. Tasaka, and Y. Takeuchi, Radioisotopes **59**, 29 (2010).
[23] S. Lindemann, PhD thesis, Heidelberg University (2013).
[24] M. Suzuki, Carbon **32**, 577 (1994).
[25] Y. Nakano, K. Ichimura, H. Ito, T. Okada, H. Sekiya, Y. Takeuchi, S. Tasaka, and M. Yamashita, Prog. Theor. Exp. Phys. **2020**, 113H01 (2020).
[26] Y. J. Cho, W. S. Cho, and S. S. Choi, Mater. Technol., **55**, 571 (2021).
[27] Y. Nakano, H. Sekiya, S. Tasaka, Y. Takeuchi, R. A. Wendell, M. Matsubara, and M. Nakahata, Nucl. Instrum. Meth. A **867**, 108 (2017).
[28] Y. Nakano, T. Hokama, M. Matsubara, M. Miwa, M. Nakahata, T. Nakamura, H. Sekiya, Y. Takeuchi, S. Tasaka, and R. A. Wendell, Nucl. Instrum. Meth. A **977**, 164297 (2020).
[29] C. Mitsuda, T. Kajita, K. Miyano, S. Moriyama, M. Nakahata, Y. Takeuchi, and S. Tasaka, Nucl. Instrum. Meth. A **497**, 414 (2003).
[30] T. Iida, Y. Ikebe, T. Hattori, H. Yamanishi, S. Abe, K. Ochifuji, and S. Yokoyama, Health Phys. **54**, 139 (1998).
[31] K. D. Chu and P. K. Hopke, Env. Sci. Technol., **22**, 711 (1988).
[32] J. O. Hirschfelder, C. F. Curtiss, and R. B. Bird, Molecular Theory of Gases and Liquids (Wiley, New York, 1954), p. 1110.
[33] J. J. van Loef, Physica B+C **103**, 362 (1981).
[34] Daiichi Kagaku Inc., Humidity calculation 1 (available at https://www.daiichi-kagaku.co.jp/situdo/note/arekore08, date last accessed May 1, 2021).